Silicon (2022) 14:9111–9116
https://doi.org/10.1007/s12633-022-01678-8

ORIGINAL PAPER

Structural, Morphological, and Gamma Ray Shielding (GRS) Characterization of HVCMC/PVP/PEG Polymer Blend Encapsulated with Silicon Dioxide Nanoparticles

Karar Abdali[1]

Received: 18 November 2021 / Accepted: 6 January 2022 / Published online: 22 January 2022

Abstract
Polymer blends and composites (PB and PCs) are novel class of developed materials which performance in the field of radiation preservation has been approved practically. The essential aim of this research is to estimate the influence of silica dioxide (SiO_2) nanoparticles (NPs) additives on the radiation shielding properties of high viscosity carboxymethyl cellulose HVCMC, poly (N-vinyl pyrrolidone) PVP and polyethylene glycol PEG polymer blend (PB). In the present paper, HVCMC/PVP/PEG PB with 0, 0.015, 0.03 and 0.045 wt% of SiO_2NPs were made using Petri dish casting method as a nanocomposites (NCs). The samples were labeled as k0,k1,k2 and k3 depending to HVCMC/PVP/PEG portions with SiO_2NPs. Structural includes X-ray diffraction (XRD), Fourier transformation infrared (FTIR) and optical microscopy (OM) were characterized. The attenuation coefficients were also calculated using caesium-137 (Cs^{137}, 662 keV) and cobalt-60 (Co^{60}, 1173 and 1332 keV) sources. Results referred that increasing of SiO_2NPs from 0% to 0.045% leads to raise in the values of attenuation coefficient and decrease the (N/N_o) values, furthermore 0.045% of SiO_2NPs doped is the ultimate optimum contain of this addition. While, the important effect on GRS characterizes happened within k3 sample for each Cs^{137} and Co^{60} radiation sources.

Keywords HVCMC · Attenuation coefficients · Gamma ray shielding · SiO_2NPs

1 Introduction

In the last years, application of PCs as the preservative shield versus GR, is very common. Radiation is energy that brings from a source and transport over space and can break through various materials. Radiation can be classified into two main groups based on its energy to ionize matter [1]. The usage of GR is speedy growing in various sectors such as industries, nuclear and atomic reactors, medicinal diagnostics, nuclear research institution, food radiance, biological researches, detecting of defects in metal and physiotherapy [2]. Scientists have studied various GRS materials in order to protect life from the degrading consequences that arise from radiation exposure while attenuating undesirable radiation [3–7]. The space, weight, cost and attenuation capacity of materials applied for GR preservation are key issues that scientists challenge to fabricate and develop suitable GR materials. Good radiation preservation is one that can attenuate, absorbs most of the incident GR [7]. HVCMC is water soluble polymer, nontoxic polysaccharide, renewable and biocompatible. HVCMC can be synthesized from a paste-same liquid of HVCMC in water by the application of GR [8, 9]. PVP is a white suspension with a type of homopolymers, stable at different temperatures, water soluble and hygroscopic polymer. Its brittle, transparent, and glassy [10, 11]. PEG from polyether has many applications in water treatment, cosmetics, medicine and industries [11, 12]. SiO_2 is an amorphous structure substance used as a dielectric in capacitors and transistors, as well as an insulator to isolate different electronic devices and as a structural layer in several micromachining operations. SiO_2 is GRS material [13].

✉ Karar Abdali
aaazezphys@gmail.com

[1] Ministry of Education, Baghdad, Iraq

2 Experimental Section

2.1 Materials

Three raw materials were purchased from Central Drug House (CDH) and used without modification: HVCMC powder (99.9%purity) with an average molecular weight Mw of (700000), PVP powder (99% purity) with Mw of (40000), PEG powder (99.8% purity) with Mw of (20000). The SiO_2 (99.8% purity) was purchased from Sigma Aldrich, with an average molecular weight of (20–30) nm. Table 1. illustrate the structure and chemical formula of all materials.

2.2 Synthesis of Nanocomposites

The PCs films were prepared by using solution casting method. HVCMC, PVP and PEG (70/20/10)wt.% were dissolved in (30 mL) deionized water (DIW). The mixture was then stirred for 55 min using a magnetic stirrer, and maintained at a temperature of around 50 °C. In the incorporation process, (0.0, 0.15, 0.30 and 0.45) wt.% from SiO_2NPs were added to the homogenous solution in steps of 0 to 40 mL. To homogenize these solutions, stirring was conducted for around 30 min. Afterward, these solutions were casted in (4 cm) Petri dishes and left to cool down at room temperature for seven days. The thickness of PB and PCs films was estimated to be between 0.080 and 0.095 cm. The ratios of PB to SiO2NPs wt.% were listed in Table 2.

2.3 XRD Patterns

XRD was used to examine the created phases. It was executed on an XR diffractometer (x'pert high score 2008, Cu k_α target radiation, wavelength = 1.5404 Å, voltage = 45 kV, current = 50 mA). The scanned data was calculated between 5° and 50°.

2.4 Fourier Transformation Infrared

To calculate the nature of the interaction between the composite materials, FTIR Vertex 701, Bruker spectrophotometer was used in the range between 400 to 4000 cm^{-1}.

Table 2 (HVCMC/PVP/PEG)/SiO_2NPs weight percentages

Sample code	wt.%			
	HVCMC	PVP	PEG	SiO_2NPs
k0	0.7000	0.200	0.1000	0.00
k1	0.6895	0.197	0.0985	0.015
k2	0.6790	0.194	0.097	0.03
k3	0.6685	0.191	0.0955	0.045

2.5 Optical Microscopy

Micro graphical images were characterized using Nikon Olympus 73,346.

2.6 GR System

The N/No values were practically computed by IEC. PTY. Geiger system rate meter with efficiency of source =5 μCi, V = 440 V, t = 100 s and No = 33 count/100 s.

3 Results and Discussion

3.1 XRD Analysis

Figure 1 includes the XRD peaks of PB and PCs films. The XRD chart of HVCMC/PVP/PEG raw materials of introduces one broad peaks characterize the semi crystalline structure of PB at 2θ of 29°. SiO_2NPs insertion leads to a

Table 1 The chemical characterizations of materials

Material	Chemical formula	Chemical structure	Ref.
HVCMC	[C6H7O(OH)3−x(OCH2COOH)x]n	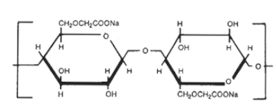	[9]
PVP	$(C_6H_9NO)_n$	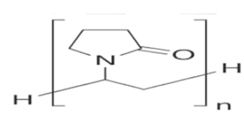	[10]
PEG	$C_{2n}H_{4n+2}O_{n+1}$	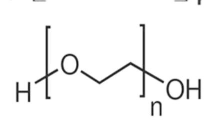	[11]
SiO_2NPs	SiO_2	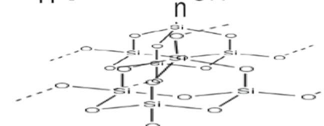	[13]

important decline in peak intensity because to the interaction which happened between the PB and SiO_2NPs. Furthermore, SiO_2NPs injection is found by the appearance of a sharp peak at 2θ of 19.4°. The Bragg reflection patterns occurring at 2θ = 29° (101), and 19.4° (211) are known for the tetrahedral structure of SiO_2NPs. The peaks of SiO_2NPs have been compared with [14], and without any phase shift. The rest of the SiO_2NPs described peaks are invisible because the small amount of SiO_2NPs over the PB. XRD peak detects a barely noticed increase of the crystalline nature with increasing SiO_2NPs content.

3.2 FTIR Spectra

The specific chemical functional groups of HVCMC/PVP/PEG blend with various SiO_2NPs contents were showed in Fig. 2. and Table 3. Figure 2,ko offers broadband peak at 3420.67 cm^{-1} of O–H stretching [15, 16], whereas the C–H stretching broadband showed at 2883 cm^{-1} [17–19]. The C=O bond is referred to the sharp band at 1649 cm^{-1} [20]. The broadband peak located at 1421.76 cm^{-1} reflects the methyl bending band [21]. The peak situated at the 1286 cm^{-1} reflects the CH_2–OH,CH_3 stretching bonds [21]. The advanced bands approved the consistence of HVCMC/PVP/PEG blend, while the insertion of SiO_2NPs lead to increasing in sharpness of peaks, exceptionally O-H, C-H and C=O peaks because to network disposal between SiO_2NPs and PB oxygenated groups. Furthermore, SiO_2NPs content caused a minor variation in the peak location of FTIR. There is no necessary variance in raw material chemical structure after doping as reported in [22]. In addition, there are new broadband peaks

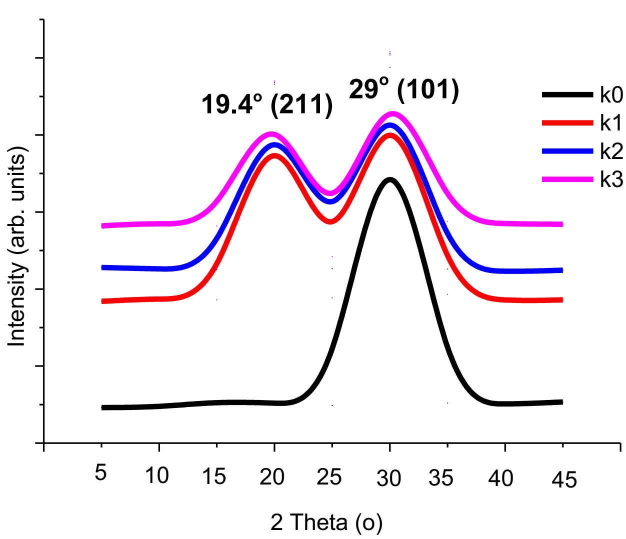

Fig. 1 XRD pattern of HVCMC/PVP/PEG blends with various SiO_2NPs contents

caused via the C=O stretching bond at 1340 cm^{-1} and transmittance peaks caused by the C-N stretching at 1105 cm^{-1},1103 and 1102 cm^{-1}, which indicate that SiO_2NPs are successfully encapsulated. The difference is which the absorption peak at 840 cm^{-1} and 959 cm^{-1} becomes a single peak related to C=C bending [22].

3.3 Surface Morphology

Figure 3 represents the morphological images of PB and PCs films at magnification power of 40X. Figure 3-ko exhibits that the HVCMC/PVP/PEG PB has homogenous and acceptable dissolving. The k1, k2, and k3 images in the same Figure indicate to the propagation of SiO_2NPs in the PB. SiO_2NPs were good diffused in the blends. The images show that no any agglomeration happened in the PCs films. The prove of which related to the interaction that absent between the raw materials and SiO_2NPs. The micrographical images refer that the uniformity of the surface was increased after loading because of the network or cross linking formed between raw material and SiO_2NPs. The OM images were good applicable with previous OM results reported in [23]. The amorphous property of surfaces were enhanced after loading.

3.4 Application of (HVCMC/PVP/PEG)/SiO_2NCs in GRS

The nature of interaction between GR and matters is a climacteric case to investigate the calculation of the capability of these radiations to propagate and fissure in the mediums which due to the technique of reaction assists to select the more usable GRS. Matters which are assumed to be applied as shields versus GR must have higher atomic number, Z and thickness. Some matters assess a higher chance of interactions which denote largest energy transport with GR [24]. Materials with lower-Z and density can industrialize of increased thickness as importantly as high-Z matters in radiation preservation [25, 26]. The PB and NCs display hopeful appropriate alternate elect to concrete and lead in the field of GR according to its durability, lightweight, elasticity along with excellent mechanical, physical, optical, and GRS characteristics [27, 28]. PBs can readily be encapsulated with various amounts of high-Z materials to create their PCs which are more respective GRS [29]. The number of counts (N) were computed via Geiger system with efficiency of radiation source (η) =5 μCi, voltage (V) = 440 V and time of count (t) = 100 s. The count of background radiation (No) was 33 counts for each 100 s. The distance between the GR source and NCs films was

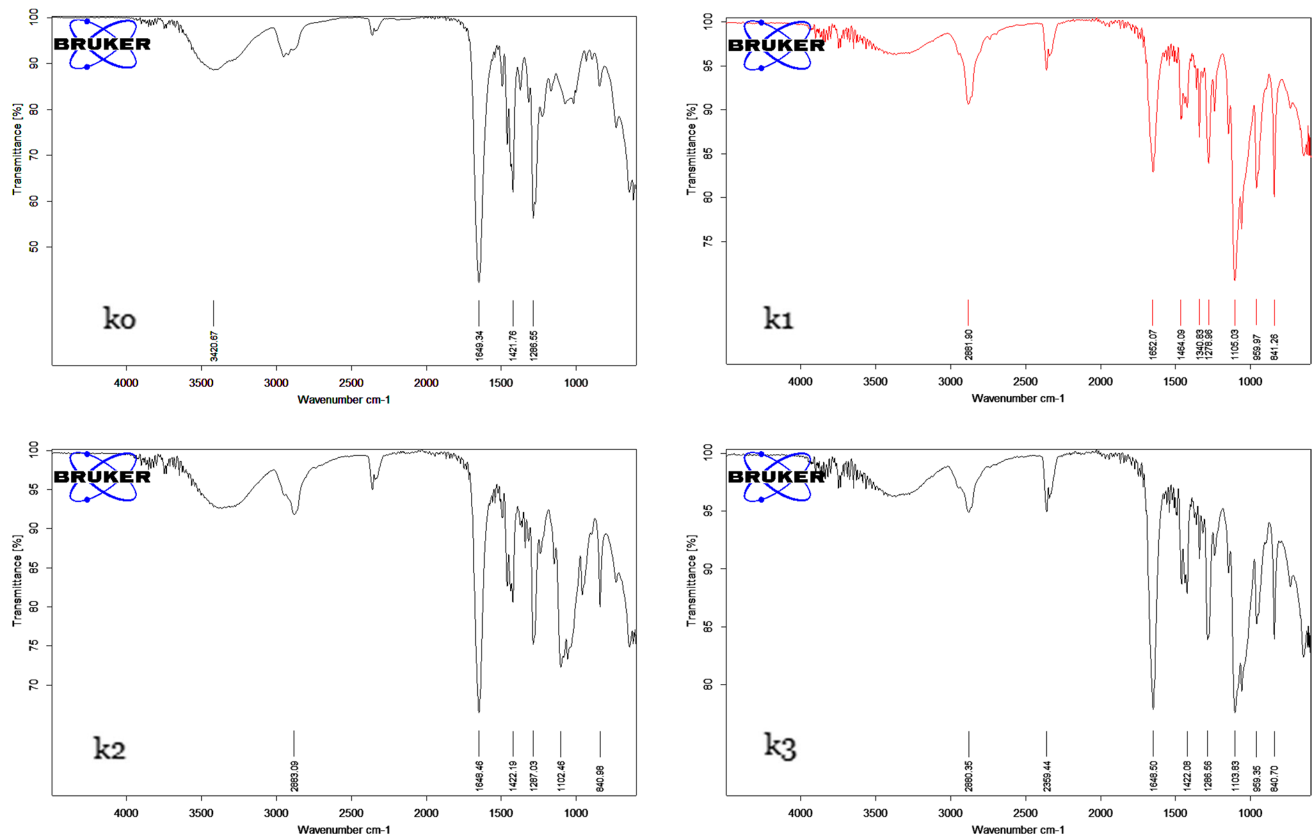

Fig. 2 FTIR spectrum of ko, k1, k2 and k3 specimens

5 cm. The distance between the detector and NCs films was 10 cm. Each N values were respectively divided on the No. Figure 4 offers that the values of N/No decreased with the increasing of SiO_2NPs contents. The (N/No) values of Cs^{137} source were greater than Co^{60}, due to the dependence of GRS on the Z, mass number (A) and thickness. The NCs films were blocked most of GR. The attenuation coefficient values of PB and NCs films were theoretically calculated by radioactivity equation as shown in Fig. 5. These values increased with increasing of SiO_2NPs, this is because the NPs effectively reflected or absorbed the GR. Furthermore, SiO_2NPs occupied a high surface area in small volume. These results exhibit a very close results if comparing with the attained results via PCs with concrete, furthermore, PCs have an characteristic over concrete due to of its minimum electrical conductivity, mobility characterizes and the ability to prevent GR shot [30, 31]. The addition of SiO_2NPs enhances the mechanical properties of raw materials such as compressive strength, density and linear attenuation coefficient and make it more suitable for using in GRS.

4 Conclusion

Novel, low cost, eco-friendly (HVCMC/PVP/PEG)-SiO_2NPs PCs films were successfully prepared via casting method. The XRD of raw materials of introduces one peaks indicate the semi crystalline structure of the PB at 2θ of 29°. The NPs doping leads to an important decline in peak sharpness related to the interaction between the raw material and SiO_2NPs contents. SiO_2NPs capsulation was detected by the appearance of a sharp peak at 2θ of 19.4°. FTIR peaks refer to appear a new broadband peaks after doping by SiO_2NPs. Furthermore, many interactions were happened between the raw material and NPs. The OM images showed that a strong and good diffusion of SiO_2NPs in the blends. The GRS results indicate that the values of N/No decrease with increasing of SiO_2NPs contents. The radiation shielding efficiency of Cs^{137} was greater than Co^{60}. The attenuation coefficient values were increased with increasing of SiO_2NPs. These results make the NCs films are suitable for using in GRS application.

Table 3 Characteristics bands of ko, k1, k2 and k3 specimens

k0	k1	k2	k3	Assignment	Ref.
3420.67	–	–	–	Stretching formula of O–H	[15, 16]
–	2881.90	2883.09	2880.35	C–H stretching formula	[17–19]
1649.34	1652.07	1648.46	1648.50	Stretching vibration of C=O	[20]
1421.76	1464.09	1422.19	1422.08	Methyl bending band	[21]
1286.55	1278.96	1287.03	1286.56	CH_2–OH,CH_3	[21]
–	1105.03	1102.46	1103.83	C-N stretching	[22]
–	959.97	–	959.35	C=C bending	[22]
–	841.26	840.98	840.70	C=C bending	[22]

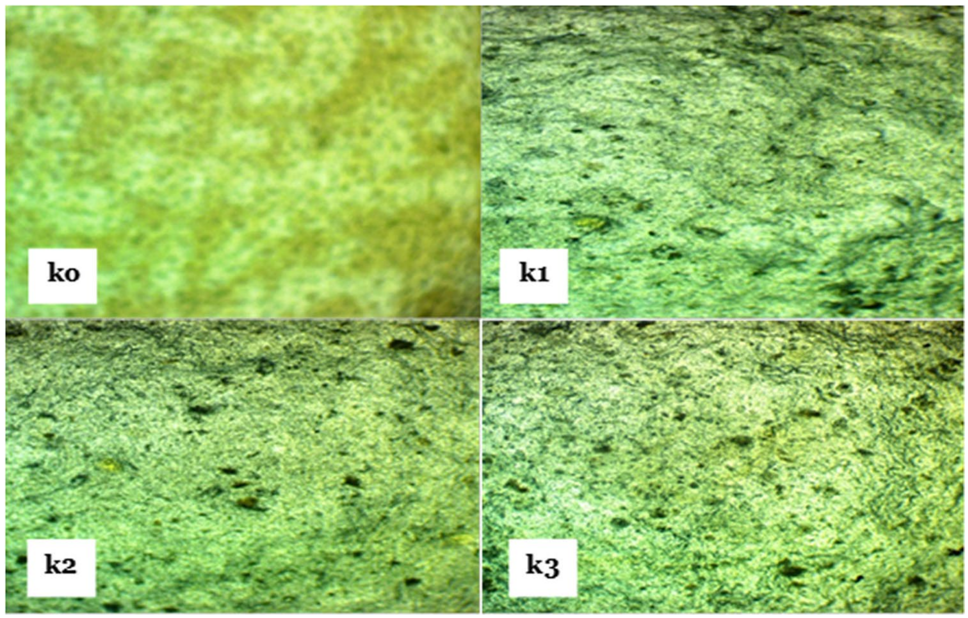

Fig. 3 Morphological images of ko, k1, k2 and k3 specimens

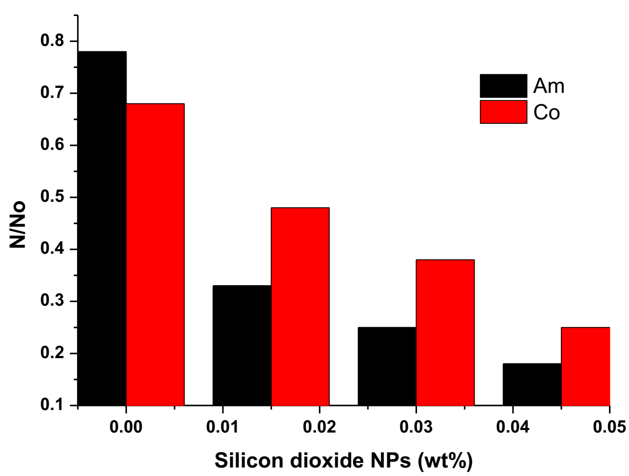

Fig. 4 N/N0 counts of ko, k1, k2 and k3 specimens

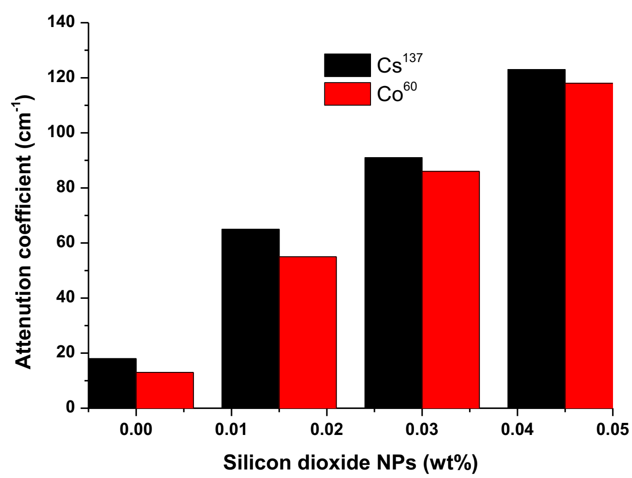

Fig. 5 Attenuation coefficient of ko, k1, k2 and k3 specimens

Supplementary Information The online version contains supplementary material available at https://doi.org/10.1007/s12633-022-01678-8.

Authors' Contributions Not applicable.

Data Availability Not applicable.

Declarations

Consent to Participate Not applicable.

Consent for Publication Not applicable.

Conflict of Interest Not applicable

References

1. Chaitali V, Zainab A, Mohamed S, Abouzeid A, Pravina P (2021) Polymeric composite materials for radiation shielding: a review. Environ Chem Lett 19:2057–2090
2. Sayyed M, Lakshminarayana G, Kityk I, Mahdi M (2017) Evaluation of shielding parameters for heavy metal fluoride based tellurite-rich glasses for gamma ray shielding applications. Radiat Phys Chem 139:33–39
3. Singh V, Badiger N, Chanthima N, Kaewkhao J (2014) Evaluation of gamma-ray exposure buildup factors and neutron shielding for bismuth borosilicate glasses. Radiat Phys Chem 98:14–21
4. Al-Buriahi M, Singh V, Arslan H, Awasarmol V, Tonguc B (2020) Gamma-ray attenuation properties of some NLO materials: potential use in dosimetry. Radiat Environ Biophys 59:145–150
5. Levet A, Kavaz E, Özdemir Y (2020) An experimental study on the investigation of nuclear radiation shielding characteristics in iron-boron alloys. J Alloys Compd 819
6. More C, Pawar P, Badawi M, Thabet A (2020) Extensive theoretical study of gamma-ray shielding parameters using epoxy resin-metal chloride mixtures. Nucl Technol Radiat Prot 35:138–149
7. Rani N, Vermani Y, Singh T (2020) Gamma radiation shielding properties of some bi-Sn-Zn alloys. J Radiol Prot 40:296–310
8. Fei B, Wach R, Mitomo H, Yoshii F, Kume T (2000) Hydrogel of biodegradable cellulose derivatives. I. Radiation-induced crosslinking of HVCMC. J Appl Polym Sci 78:278–283
9. Wach R, Mitomo H, Yushii F, Kume T (2001) Hydrogel of biodegradable cellulose derivatives. II. Effect of some factors on radiation-induced crosslinking of HVCMC. J Appl Polym Sci 81:3030–3037
10. Jenkins A (1972) Polymer science, a material science handbook. American Elsevier Publishing Company. 12: 428–432
11. James E (1999) Polymer Data Handbook. Oxford University Press. 2: 962–964
12. Karar A, Lamis F, Alhak A, Abdulazeez O, Ali A (2018) Enhancing some physical properties of cosmetic face powders. Journal of Global Pharma Technology 10:75–78
13. Michael L, Gary K (1998) In handbook of sensors and actuators. Science Direct 6:1–268
14. Waseem M, Mustafa S, Naeem A, Shah K, Shah I, Haque I (2009) Synthesis and Charactraization of silica by sol-gel method. J Pak Mater Soc 3:19–21
15. Rahmani H, Najafi S, Ashori A, Fashapoyeh M, Mohseni F, Torkaman S (2020) Preparation of chitosan-based composites with urethane cross linkage and evaluation of their properties for using as wound healing dressing. Carbohydr Polym 230
16. Elashmawi I, Menazea A (2019) Different time's Nd:YAG laser-irradiated PVA/ag nanocomposites: structural, optical, and electrical characterization. J Mater Res Tech 8:1944–1951
17. Zhong Z, Qin J, Ma J (2015) Cellulose acetate/hydroxyapatite/chitosan coatings for improved corrosion resistance and bioactivity. Mater Sci Eng C Mater Bio Appl 49:251–255
18. Shakir M, Jolly R, Khan M, Iram N, Khan H (2015) Nanohydroxyapatite/chitosan-starch nanocomposite as a novel bone construct: synthesis and in vitro studies. Int J Biol Macromol 80:282–292
19. Mohammad A, Salah-Eldin T, Hassan M, El-Anadouli B (2017) Efficient treatment of lead-containing wastewater by hydroxyapatite/chitosan nanostructures. Arab J Chem 10:683–690
20. Zhao H, Jin H, Cai J (2014) Preparation and characterization of nano-hydroxyapatite/chitosan composite with enhanced compressive strength by urease-catalyzed method. Mater Lett 116:293–295
21. Nagireddi S, Katiyar V, Uppaluri R (2017) Pd(II) adsorption characteristics of glutaraldehyde cross-linked chitosan copolymer resin. Int J Biol Macromol 94:72–84
22. Elabbasy M, Ahmed M, Menazea A (2021) Structural, morphological features, and antibacterial behavior of PVA/PVP polymeric blends doped with silver nanoparticles via pulsed laser ablation. J Mater Res Technol 13:291–300
23. Habeeb M, Abdul-Hamza R (2018) Novel of (biopolymer blend-MgO) nanocomposites: fabrication and characterization for humidity sensors. J Bionanosci 12:328–335
24. Chang L, Zhang Y, Liu Y, Fang J, Luan W, Yang X, Zhang W (2015) Preparation and characterization of tungsten/epoxy composites for γ-rays radiation shielding. Nucl Instrum Methods Phys Res B 356:88–93
25. Luković J, Babić B, Bučevac D, Prekajski M, Pantić J, Baščarević Z, Matović B (2015) Synthesis and characterization of tungsten carbide fine powders. Ceram Int 41:1271–1277
26. Mostafa A, Issa S, Sayyed M (2017) Gamma ray shielding properties of PbO-B_2O_3-P_2O_5 doped with WO_3. J Alloys Compd 708:294–300
27. Rani N, Vermani Y, Singh T (2020) Gamma radiation shielding properties of some bi-Sn-Zn alloys. J Radiol Prot 40:296–310
28. Alavian H, Tavakoli H (2020) Comparative study of mass attenuation coefficients for LDPE/metal oxide composites by Monte Carlo simulations. Eur Phys J Plus 135:82
29. Atashi P, Rahmani S, Ahadi B, Rahmati A (2018) Efficient, flexible and lead-free composite based on room temperature vulcanizing silicone rubber/W/Bi_2O_3 for gamma ray shielding application. J Mater Sci Mater Electron 29:10
30. Majeed A, Waleed S (2019) Characterization of (CMC-PVP-Fe_2O_3) nanocomposites for gamma shielding application. IJETER. 7:247–255
31. Eltohamy R, Mosad M (2016) Effect of gamma ray energies and addition of Nano- SiO_2 to cement on mechanical properties and mass attenuation coefficient. IOSR-JMCE. 13:17–22

Publisher's Note Springer Nature remains neutral with regard to jurisdictional claims in published maps and institutional affiliations.